Published in final edited form as:
Traffic. 2011 October ; 12(10): 1341–1355. doi:10.1111/j.1600-0854.2011.01234.x.

Osh proteins regulate membrane sterol organization but are not required for sterol movement between the ER and PM

Alexander Georgiev[1], **David P. Sullivan**[1,3], **Michael C. Kersting**[1], **Jeremy S. Dittman**[1], **Christopher T. Beh**[2], and **Anant K. Menon**[1,†]

[1]Department of Biochemistry, Weill Cornell Medical College, New York, NY, USA

[2]Department of Molecular Biology and Biochemistry, Simon Fraser University, Burnaby, British Columbia, Canada

Abstract

Sterol transport between the endoplasmic reticulum (ER) and plasma membrane (PM) occurs by an ATP-dependent, non-vesicular mechanism that is presumed to require sterol transport proteins (STPs). In *Saccharomyces cerevisiae*, homologues of the mammalian oxysterol-binding protein (Osh1–7) have been proposed to function as STPs. To evaluate this proposal we took two approaches. First we used dehydroergosterol (DHE) to visualize sterol movement in living cells by fluorescence microscopy. DHE was introduced into the PM under hypoxic conditions and observed to redistribute to lipid droplets on growing the cells aerobically. Redistribution required ATP and the sterol acyltransferase Are2, but did not require PM-derived transport vesicles. DHE redistribution occurred robustly in a conditional yeast mutant (*osh*Δ *osh*4-1^{ts}) that lacks all functional Osh proteins at 37°C. In a second approach we used a pulse-chase protocol to analyze the movement of metabolically radiolabeled ergosterol from the ER to the PM. Arrival of radiolabeled ergosterol at the PM was assessed in isolated PM-enriched fractions as well by extracting sterols from intact cells with methyl-β-cyclodextrin. These experiments revealed that whereas ergosterol is transported effectively from the ER to the PM in Osh-deficient cells, the rate at which it moves within the PM to equilibrate with the methyl-β-cyclodextrin extractable sterol pool is slowed. We conclude (i) that the role of Osh proteins in nonvesicular sterol transport between the PM, ER and lipid droplets is either minimal, or subsumed by other mechanisms and (ii) that Osh proteins regulate the organization of sterols at the PM.

Keywords

cholesterol; cyclodextrin; ergosterol; dehydroergosterol; detergent resistant membrane; endoplasmic reticulum; lipid droplet; lipid transfer protein; Osh protein; oxysterol-binding proteins; non-vesicular transport; plasma membrane; yeast

Sterols, such as cholesterol in mammalian cells and ergosterol in fungi (Fig. 1A), are important components of biological membranes (1). They are highly enriched in the plasma membrane (PM)[1](2–5). For example, the PM of the budding yeast *Saccharomyces cerevisiae* contains ~10^8 ergosterol molecules, corresponding to ~40 mole percent of total

†Correspondence to: Anant K. Menon; akm2003@med.cornell.edu.
[3]Present address: Department of Pathology, Northwestern University, Feinberg School of Medicine, Chicago, IL, USA

[1]**Abbreviations used:** ALA, 5-aminolevulinic acid; CERT, ceramide transport protein; DHE, dehydroergosterol; DRM, detergent resistant membrane; ER, endoplasmic reticulum; LD, lipid droplet; ORD, OSBP-related domain; OSBP, oxysterol-binding protein; PM, plasma membrane; StAR; steroidogenic acute regulatory protein; START, StAR-related lipid transfer; STP, sterol transport protein

PM lipids and ~70% of total cellular ergosterol (6–8). Ergosterol is synthesized in the endoplasmic reticulum (ER) and transported to the PM primarily by an ATP-requiring, non-vesicular mechanism (9, 10) (Fig. 1B). Retrograde transport also occurs, since exogenously supplied sterols can move from the PM to the ER where they are esterified by sterol acyl transferase enzymes Are1 and Are2 and encapsulated in lipid droplets (LDs)(11, 12) (Fig. 1B).

The non-vesicular transport of sterols between the ER and PM is poorly understood (13). Because sterols are largely insoluble in water, they must be shielded from the aqueous environment for transport to occur efficiently. In analogy with other lipid transport processes, this is likely to require a cytoplasmic lipid transport protein similar to the ceramide transport protein (CERT)(14) and the steroidogenic acute regulatory protein (StAR)(15, 16). The former catalyzes ATP-dependent, non-vesicular transport of ceramide from the ER to the Golgi, whereas the latter is involved in transporting cholesterol to the inner mitochondrial membrane. These proteins are presumed to extract lipids from a donor membrane, shield them during transport through the aqueous milieu of the cytoplasm and offload them when encountering an acceptor membrane. Transport is bi-directional (Fig. 1B) and so there is no net flux unless the lipid is consumed at the acceptor membrane (4).

Sterol transport proteins (STPs) required for ER-PM sterol transport have not been identified. Budding yeast lack CERT and StAR homologues, but they possess seven homologues (Osh1–7) of the mammalian oxysterol-binding protein [OSBP] that have been proposed to function as STPs (17–19) (Fig. 1C). Although no single Osh protein is essential, and any one can substitute for the other six, disruption of all seven *OSH* genes is lethal (20). This suggests that Osh proteins have a common essential function. X-ray crystallographic analyses of Osh4 (also known as Kes1) show that it has a deep lipid-binding pocket covered with a regulatory flap that could open when the protein is membrane associated (19). The lipid-binding pocket accommodates a single sterol molecule, with its hydroxyl group pointing toward the bottom of the pocket(19). Based on this structural model it was suggested that Osh4 could extract sterol from one membrane, sequester it in its lipid-binding pocket, and offload it at another membrane (19). Consistent with this idea, Osh4, Osh5 and Osh2-ORD (the OSBP-related domain of Osh2) were shown to transport sterols between populations of liposomes (18, 21), and the retrograde transport of cholesterol was shown to be 7-fold slower in Osh-deficient yeast cells (18). Thus, the common essential function of Osh proteins could be to transport sterols between the ER and PM.

To test this hypothesis, we compared sterol trafficking in wild-type cells and cells lacking functional Osh proteins. We introduced dehydroergosterol (DHE), a naturally occurring fluorescent sterol (22, 23), into the PM and observed its redistribution to LDs by fluorescence microscopy. Redistribution of DHE to LDs was correlated with the production of DHE esters. In the second approach we generated a pulse of radiolabeled ergosterol in the ER and monitored its arrival at the PM by measuring radioactivity in PM-enriched subcellular fractions and detergent resistant membranes (DRMs), as well as in the sterol fraction extracted from intact cells by methyl-β-cyclodextrin (MβCD). Our results indicate that (i) Osh proteins are dispensable for sterol movement between the PM, ER and LDs, and (ii) Osh protein family members regulate the organization of sterols at the PM.

RESULTS

DHE can functionally replace yeast ergosterol

DHE is a naturally occurring sterol, similar to yeast ergosterol and mammalian cholesterol (Fig. 1A). To validate its use as a fluorescent reporter of intracellular ergosterol transport in living yeast cells, we tested whether DHE could functionally replace ergosterol. To facilitate

DHE uptake into yeast, we made use of the sterol auxotrophy of cells that are unable to synthesize heme. The enzyme 5-aminolevulinate synthase, encoded by *HEM1*, catalyzes the first step in the heme biosynthetic pathway (24); *hem1*Δ strains can grow in media that is supplemented with 5-aminolevulinic acid (ALA), but in the absence of ALA a sterol supplement is required (25). DHE supported the growth of *hem1*Δ cells as effectively as ALA or ergosterol (Fig. 1D). After shifting ALA-grown *hem1*Δ cells to DHE-containing media for 48 hrs,>99% of the cellular sterol was DHE (Table 1). The DHE content of these cells (per OD_{600} unit) was similar to the ergosterol content of a parallel culture grown with an ergosterol supplement (Table 1). We conclude that DHE can replace the bulk function of ergosterol *in vivo* and is therefore a suitable probe for the study of intracellular ergosterol traffic in yeast. A similar conclusion was recently reported (26).

DHE is incorporated into the PM of hypoxically grown yeast

Under normal growth conditions, yeast cells cannot import exogenously supplied sterols, a phenomenon termed `aerobic sterol exclusion', and rely entirely on ergosterol biosynthesis to meet their sterol requirements (27). However, because ergosterol biosynthesis requires molecular oxygen, yeast cells grown under hypoxic or anaerobic growth conditions must import sterols to maintain viability (28). The ability to import sterols depends on the PM-localized ABC transporters Aus1 and Pdr11 (Fig. 1B) that are expressed only when oxygen levels are low (29).

We exploited the ability of yeast cells to take up sterols under hypoxic conditions to introduce DHE into the PM. We supplemented a yeast culture with DHE and incubated the cells for 36 hrs at 30°C in <0.7% (v/v) oxygen. When the cells were examined by fluorescence microscopy, a uniform signal was detected at the cell cortex, indicating PM-localized DHE (Fig. 2A)(26). No fluorescence was observed in cultures incubated with ergosterol instead of DHE, indicating that the fluorescence we observed was due to DHE rather than cellular autofluorescence (Fig. 2B). As expected, hypoxic conditions were necessary for DHE incorporation, because no cell-associated fluorescence was observed in cultures that were grown aerobically in the presence of DHE. Reversed phase HPLC analysis established that fluorescence was due to DHE and not a metabolite such as DHE ester (Fig. 2C). About 80% of the total cellular sterol was recovered as DHE, with the rest being ergosterol (Table 1).

We confirmed the PM localization of DHE by Renocal gradient fractionation of a yeast cell homogenate. This procedure separates the PM from the ER and other organelle membranes(30). Consistent with the normal distribution of endogenous ergosterol, DHE levels were highest in gradient fractions containing the PM marker Gas1 and uniformly low in fractions containing the ER marker Sec61 (Fig. 2D). The low DHE content of the Sec61-containing fractions indicates that high DHE levels in the PM fraction are unlikely to be due to contamination of that fraction with cortical ER.

Redistribution of DHE from the PM to LDs

To visualize sterol trafficking from the PM, cells were loaded with DHE as described above, and then incubated aerobically for 1 hr at 30°C prior to examination by fluorescence microscopy. Fluorescence was seen to be entirely intracellular, occupying a number of discrete foci that co-localized with the LD markers Nile Red (Fig. 3A) and Erg6 (not shown).

HPLC analyses of lipid extracts prepared from the cells revealed that a significant percentage (~40%) of DHE had been converted to DHE esters (Fig. 3B), consistent with localization of fluorescence to LDs. Furthermore, no intracellular foci were seen in

*are1*Δ*are2*Δ double mutant cells that lack the ability to esterify sterols. Examination of the single mutants *are1*Δ and *are2*Δ suggested that esterification under these conditions was primarily due to Are2 which is the major catalytic isoform (31, 32)(Fig. 3C, top panels).

DHE redistribution is likely linked to the initiation of ergosterol biosynthesis as oxygen becomes available (33). Thus, we propose that newly synthesized ergosterol displaces DHE at the PM, resulting eventually in its esterification and sequestration in LDs. Consistent with this proposal, cellular ergosterol content increased ~6-fold, from ~140 ± 80 pmol (per OD_{600} unit of cells) at time zero to 840 ± 165 pmol after the 60 min aerobic incubation period.

Several experiments established the characteristics of DHE redistribution from the PM to LDs. If the samples were kept on ice or treated with energy poisons immediately after DHE loading, the PM fluorescence pattern persisted for several hours and no intracellular foci were observed (Fig. 3D). We examined DHE redistribution in *end4-1*^{ts} cells that are defective for endocytosis at 37°C (34). Whereas transport of the lipid dye FM4–64 (35) from the PM to vacuoles was blocked in these cells at 37°C as expected (not shown), redistribution of DHE from the PM to intracellular foci was not (Fig. 3C, bottom panels). Thus, redistribution of DHE from the PM to LDs does not require vesicular transport from the PM. Our data suggest that a fraction of DHE moves from the PM to the ER during the aerobic incubation period. At the ER, it is esterified by Are2 and packaged into LDs. The overall redistribution process occurs by a non-endocytic mechanism that requires metabolic energy. The molecular basis of the metabolic energy requirement is unknown: energy may be required directly for transport, *e.g.*, to activate an STP by phosphorylation, or indirectly for the assay read-out, *e.g.*, synthesis of fatty acyl CoA for steryl ester production.

Kinetics of DHE redistribution

To evaluate the rate at which DHE redistributes from the PM to LDs during aerobic incubation, we analyzed samples taken at different time points over a 60-min period. The samples were preserved for analysis by adding energy poisons and incubating on ice. Three complementary analyses were performed.

First, fluorescence images were recorded and scored manually by binning the fluorescence pattern into three categories: PM-staining, intracellular foci and an intermediate category (Fig. 4A,B). More than 200 cells were scored per time-point. Data compiled from 3 independent experiments are shown in Fig. 4B. The results reveal that DHE fluorescence begins to disappear from the cell periphery immediately on shifting the cells to aerobic conditions and starts to be detectable in intracellular foci after a lag period of ~20 min. The entire redistribution process is complete by ~60 min as assessed by this method (Fig. 4B).

We also prepared lipid extracts from the cells at each time point and analyzed these by HPLC to determine the extent of conversion of DHE to DHE esters (Fig. 4C,D). These results corroborated the data obtained by fluorescence microscopy. DHE esterification commenced with a lag period of ~20 min, coincident with the appearance of intracellular fluorescent foci. However, only ~40% of the DHE was converted to DHE ester after 60 min (>70% conversion of DHE to DHE ester occurred with an incubation of 120 min) whereas manual scoring suggested that all of the observable DHE had relocated from the PM to LDs. Closer examination of the fluorescence images suggested that a significant proportion of DHE was diffusely distributed throughout cells that also had intracellular foci (Fig. 4A), accounting for the difference in the estimates obtained by manual scoring and ester analysis. We therefore assessed total intracellular DHE by an image processing protocol. We generated a mask from the DIC image of each cell, and used it to define fluorescence at the cell cortex and within the cell interior (Fig. 4E). Quantification of all intracellular fluorescence by this method revealed that ~25% of the DHE was intracellular at time zero

(this is likely an overestimate because of the contribution of out-of-plane fluorescence from PM-localized DHE at early time points) whereas 75% of the DHE was intracellular at the 60-min time point (Fig. 4F). Thus after 60 min, greater than half of the internalized DHE is localized in LDs in the form of DHE esters. We conclude that DHE redistributes from the PM to the cell interior during the aerobic incubation period, on a time scale of minutes, eventually localizing to LDs.

DHE redistribution occurs robustly in cells lacking functional Osh proteins

We used the DHE redistribution assay to test the hypothesis that Osh proteins are required for sterol transport between the PM, ER and LDs. Because yeast cells require the expression of at least one member of the Osh protein family for viability, we used a haploid strain (*osh*Δ *osh4-1*^{ts}) that lacks all seven chromosomally encoded Osh proteins but contains a plasmid expressing a temperature-sensitive Osh4 mutant in which a glycine residue (G183) is replaced with aspartic acid (36). At 23°C the *osh4-1* allele is functional ensuring cell viability at ambient temperature, but it is non-functional at 37°C. Figure 5A shows that the temperature-sensitive growth phenotype of this strain is preserved under hypoxic conditions.

We incubated *osh*Δ *osh4-1*^{ts} cells under hypoxic conditions in the presence of DHE for 36 hrs at 23°C, then shifted the temperature to 37°C for 60 min before transferring the cells to aerobic conditions at 37°C. Samples were withdrawn every 20 min and DHE redistribution was examined. Fluorescence images of cells taken at the 0 and 60-min time point (Fig. 5B) show clearly that DHE redistributes from the PM to LDs effectively in *osh*Δ *osh4-1*^{ts} cells at the non-permissive temperature indicating that Osh proteins are dispensable for this process.

Manual scoring of fluorescence images indicated that DHE redistribution occurred with similar kinetics in both *osh*Δ *osh4-1*^{ts} and wild-type cells (Fig. 5C). However, whereas both cell types showed clear fluorescent foci at the 60-min time point, the *osh*Δ *osh4-1*^{ts} cells had a higher level of diffuse fluorescence. This suggested that the rate of intracellular transport and/or esterification of DHE might be slightly reduced as a result of Osh deficiency. Analysis of fluorescence images taken at different time points revealed that intracellular accumulation of DHE occurs ~2.5-fold more slowly in the Osh-deficient strain than in wild-type cells (Fig. 5D). As indicated above, this value is an overestimate, more so as the characteristic flocculation of the Osh-deficient cells increases the contribution of out-of-plane fluorescence, especially at early time-points. We also carried out HPLC analyses to measure DHE esters. Figure 5E shows that the rate of DHE esterification is ~2-fold lower in the *osh*Δ *osh4-1*^{ts} mutant than in wild-type cells. The reduction in the rate of esterification was not due to ACAT deficiency as ACAT activity in the mutant cells was ~2-fold higher than in wild-type cells (2.13 ± 0.27 vs 0.89 ± 0.02 nmol/mg/min). We conclude that redistribution of DHE from the PM to intracellular compartments and LDs is slowed ~2-fold in the absence of the Osh proteins (Fig. 5G). This is a small effect, possibly a downstream consequence of the loss of Osh protein function. We conclude that members of this protein family are not required for direct transfer of sterols from the PM to internal membranes and, in turn, to LDs.

Transport-coupled conversion of cholesterol to cholesteryl esters in Osh-deficient cells

Our results with DHE are quantitatively different from those of Raychaudhuri et al. (18) who reported that cholesterol transport from the PM to LDs is slowed by ~7-fold in the absence of Osh proteins. Possible reasons for the difference include distinct methods of sterol loading (hypoxic conditions versus use of *upc2-1* strains), and the use of cholesterol versus DHE.

To explore the latter possibility we tested cholesterol in our uptake assay. We discovered that, different from the situation with DHE, cholesterol esterification occurs to some extent even under hypoxic conditions. We therefore incubated *osh*Δ *osh4-1*^{ts} cells under hypoxic conditions at the permissive temperature, shifted the culture to 37°C for 60 min, then incubated aerobically for 60 min at 37°C in YPD medium supplemented with [^{14}C] cholesterol. The wild-type parental strain was processed alongside. Figure 5F shows that cholesteryl esters are formed ~1.5-fold more slowly in the Osh-deficient cells compared with wild-type cells. These data reinforce the conclusions of the DHE redistribution assay (cumulative results are summarized in Fig. 5G), *i.e.*, that Osh protein deficiency has only a modest effect on retrograde transport of sterol from the PM to the ER and LDs.

The reasons for the discrepancy between our results and those of Raychaudhuri et al. are unclear. We note, however, that under our assay conditions ACAT activity is ~2-fold higher in the *osh*Δ *osh4-1*^{ts} cells than in comparably treated wild-type cells (see above) whereas Raychaudhuri et al. report that the ACAT activity of Osh-deficient (*osh*Δ *osh4-1*^{ts} *upc2-1*) cells is 2-fold lower than that of wild-type cells (18). If esterification is the rate-limiting step in the movement of sterols from the PM to LDs, then the rate of cholesterol movement from the PM to the ER would be ~3-fold (the present study) and ~3.5-fold (Raychaudhuri et al.) lower in Osh-deficient cells compared with wild-type cells, making the results of the two studies comparable.

Newly synthesized ergosterol is transported rapidly from the ER to the PM in Osh-deficient cells

We next tested whether Osh proteins play a role in moving ergosterol from the ER to the PM. For this we incubated *osh*Δ *osh4-1*^{ts} cells for 90 min at the non-permissive temperature (37°C), before pulse-labeling them with [^{3}H-methyl]-methionine for 4 min at the same temperature to generate a pool of newly synthesized [^{3}H]ergosterol in the ER. We then tracked the movement of this pool to the PM over a chase period of 90 min at 37°C. Wild-type cells were analyzed in parallel. Transport was assessed by measuring [^{3}H]ergosterol in the PM by two different methods.

1. Assay using subcellular fractionation—Cell samples were collected at the end of the pulse and chase periods, chilled, treated with energy poisons and homogenized. After low speed centrifugation to remove cell debris, the homogenate was subjected to sucrose gradient centrifugation to resolve subcellular fractions (37, 38). The protocol does not involve a prior direct pelleting of the membranes as this could conceivably facilitate ergosterol exchange through membrane contacts (39). As shown in Fig. 6A and consistent with previous reports (38), the fractionation procedure effectively resolves the PM from ER and other internal membranes (vacuole, endosomes, Golgi membranes). The PM is mainly recovered near the bottom of the gradient as indicated by the profile of ergosterol and the PM marker protein Gas1, whereas the ER fractionates in the top half of the gradient as seen by the distribution of the ER protein translocon Sec61 and the mannosyl-transferase Dpm1 (not shown). As Sec61 is known to be distributed throughout the ER, including the cortical ER region that lies adjacent to the PM (37), it is clear from Fig. 6A that the PM-enriched fractions are not contaminated by ER membranes. Fractionation profiles of *osh*Δ *osh4-1*^{ts} cells and wild-type cells were similar; also, there was no difference in the fractionation profiles of samples taken at the end of the pulse period and after a 90 min chase (the data in Fig. 6A correspond to *osh*Δ *osh4-1*^{ts} cells at the end of the 90 min chase period).

The specific radioactivity (SR = cpm ÷ absorbance units) of ergosterol was determined for subcellular fractions as well as for whole cells, and the relative specific radioactivity ($RSR_{frac} = SR_{frac} \div SR_{cell}$) of fractions pooled pairwise from the top of the gradient was

calculated. We first analyzed wild-type cells. At the end of the pulse period, ER-enriched membranes (fractions 1–10) had an RSR_{frac} >1 whereas the PM (fractions 13–14) had an RSR_{frac} <1 (Fig. 6B; blue squares). At the end of the chase period all gradient fractions had an RSR_{frac} ~1 (Fig. 6B; yellow circles). These data indicate that at the end of the labeling pulse [^{3}H]ergosterol is mainly located in the ER-enriched fractions as expected, but by the conclusion of the chase period it has equilibrated completely with the PM and other cellular membranes.

The spontaneous movement of ergosterol between membranes during the fractionation procedure is predicted to be very slow ($t_{1/2}$ >100 hr at 4°C (40, 41)) and so it is unlikely to be a factor in our analysis. Moreover, if ergosterol moved spontaneously between membranes at an appreciable rate during the fractionation procedure, then RSR_{frac} would have been equal to 1 for all fractions in the end-of-pulse sample. As RSR_{frac} is not equal to 1 in almost all fractions from the end-of-pulse sample (Fig. 6B; blue squares), it is clear that spontaneous transfer of ergosterol between membranes during this analysis is negligible.

Figure 6B shows the RSR_{frac} profiles for Osh-deficient and wild-type cells at the end of the pulse period and after a 90 min chase. The profiles at each time point are essentially the same, indicating that Osh-deficiency does not affect movement of ergosterol from the ER to the PM. Of note, RSR_{frac} of the PM (fractions 13–14) was ≥ 0.5 at the end of the pulse period for both strains indicating that the $t_{1/2}$ for ergosterol movement between the ER and PM is ≥ 4 min, irrespective of Osh protein function. It is possible that non-vesicular anterograde sterol transport - like retrograde transport (Fig. 5G) - is slightly slower in Osh-deficient cells compared with wild-type cells and that this is masked by a low level of vesicular sterol transport.

2. Assay using DRMs—We next analyzed the movement of ergosterol from the ER to the PM by exploiting the fact that newly synthesized ergosterol is largely soluble in ice-cold Triton X-100 whereas PM-localized ergosterol is found in DRMs (9, 42). In a previous report (9) we showed that the RSR of the DRM fraction ($RS_{RDRM} = SR_{DRM} \div SR_{cell}$) was ~0.5 at the end of the 4 min pulse radiolabeling period and rose to 1 by the end of a 60 min chase, consistent with movement of ergosterol from the ER to the PM. We carried out a similar analysis, comparing wild-type and Osh-deficient cells. The cells were prepared as described for the fractionation experiment except that samples withdrawn at the end of the pulse and chase periods were treated with ice-cold Triton X-100. DRMs were separated from detergent-soluble material by centrifugation. Recovery of bulk, unlabeled ergosterol was ~62.5 ± 5.4% for all samples, consistent with previous reports (9, 42). Figure 6C shows that RSR_{DRM} is ~0.5 and ~1 for the end-of-pulse and end-of-chase samples, respectively, for both wild-type and Osh-deficient cells. These data suggest that the movement of newly synthesized ergosterol from the ER to the PM, here operationally defined as the DRM fraction, does not require Osh proteins.

Transport of newly synthesized ergosterol measured by sampling PM ergosterol with MβCD

We previously described an assay in which delivery of newly synthesized [^{3}H]ergosterol to the PM was measured by sampling PM ergosterol in intact cells with MβCD (9). As non-vesicular transport exchanges lipids between the cytoplasmic leaflets of cell membranes, newly synthesized ergosterol must first be delivered to the cytoplasmic leaflet of the PM before it can move to the MβCD-accessible outer leaflet. Thus, the MβCD sampling assay measures the end result of at least two transport steps. In contrast, the fractionation-based assays described in the previous section measure delivery of [^{3}H]ergosterol to the PM as a whole and do not distinguish ergosterol pools within the PM.

To assay transport of newly synthesized synthesized ergosterol to the PM by MβCD sampling, cells were removed at different times during the chase period and incubated with MβCD on ice for 20 min. After incubation, the sample was centrifuged and the cell-free supernatant containing MβCD–bound sterols (termed `MβCD–extract') was analyzed by organic solvent extraction and HPLC to determine its content of [^{3}H]ergosterol and non-labeled ergosterol. An untreated cell sample was analyzed in parallel.

Under our standard conditions the amount of ergosterol extracted by MβCD from wild-type cells was ~0.25% of total cellular ergosterol as previously reported (9), reminiscent of the poor extractability of DHE from large unilamellar vesicles composed of phosphatidylcholine with saturated acyl chains (43). In contrast, the amount of ergosterol extracted from Osh-deficient cells under the same conditions was 6.3 ± 0.4% of total cellular ergosterol, corresponding to a ~25-fold greater extraction efficiency. The increased extractability may reflect a change in ergosterol organization at the PM in Osh-deficient cells (see Discussion).

Figure 7A shows the amount of [^{3}H]ergosterol in the MβCD-extract from wild-type and Osh-deficient cells as a function of time, corrected for the 1.7-fold lower level of [^{3}H]ergosterol synthesis in the latter. For wild-type cells, the [^{3}H]ergosterol content of the MβCD-extract increased mono-exponentially ($t_{1/2}$ ~20 min), whereas for Osh-deficient cells the amount of [^{3}H]ergosterol in the MβCD-extract increased linearly at a rate ~2.5-fold greater than the initial rate measured for wild-type cells (Fig. 7A).

If ergosterol transport (measured by MβCD sampling) occurs at the same rate in wild-type and Osh-deficient cells then the 25-fold higher efficiency of MβCD-mediated ergosterol extraction from the latter should correlate with a 25-fold increase in the initial rate at which [^{3}H]ergosterol is recovered in the MβCD-extract (Fig. 7A; compare the measured initial rate for wild-type cells indicated by the line labeled `IR wt' with that predicted for Osh-deficient cells indicated by the line labeled `IR predicted for *osh*Δ'). This is not what we observed. Instead, the experimentally measured rate of ergosterol transport for Osh-deficient cells was 10-fold lower than the predicted rate.

To facilitate comparison, the transport data (Fig. 7A) were normalized to correct for the efficiency of MβCD-mediated ergosterol extraction. This yielded a graph of the relative specific radioactivity of the MβCD-extract (RSR = $SR_{M\beta CD} \div SR_{cell}$) as a function of time (Fig. 7B), similar to graphs described in earlier publications (9, 44). It is evident from Fig. 7B that [^{3}H]ergosterol is transferred to the MβCD-extractable pool of PM sterol much more slowly in Osh-deficient cells compared with wild-type cells. These data suggest that Osh-deficiency affects either the delivery of ergosterol from the ER to the PM, or the subsequent movement of ergosterol within the PM to an MβCD-accessible location, or both.

The results from the MβCD sampling assay contrast with those obtained with the fractionation-based assay (Fig. 6C). Firstly, the timing ($t_{1/2}$) of ergosterol delivery to the PM in wild-type cells is different for the two assays: ≤ 4 min (fractionation assay) and ~20 min (MβCD sampling assay). Secondly, for Osh-deficient cells, the corresponding $t_{1/2}$ values are ≤ 4 min (as for wild-type cells) and ~200 min (10-fold slower than for wild-type cells). This suggests that ergosterol moves rapidly from the ER to the PM, then more slowly within the PM to an MβCD-accessible location. Osh proteins affect only the latter transport step. This model is presented in more detail in the Discussion.

DISCUSSION

We analyzed intracellular sterol movement in yeast using five different assays: transport of DHE and cholesterol from the PM to the ER and LDs (quantified by fluorescence microscopy and HPLC determination of steryl esters) and transport of newly synthesized

ergosterol from the ER to the PM (monitored by determining radioactivity in subcellular fractions, detergent resistant membranes and MβCD extracts). Based on these assays we conclude that Osh proteins are dispensable for the bidirectional movement of sterols between the ER and PM, but that one or more members of the Osh protein family influences sterol organization within the PM. These conclusions are discussed below.

Osh proteins are dispensable for sterol movement between the PM, ER and LDs

We describe a new assay for intracellular sterol transport in yeast that makes use of the fluorescent sterol DHE as a transport reporter. DHE, a naturally occurring sterol, functionally replaces ergosterol and under appropriate conditions, accounts for all the sterol content of the cells (Table 1). The assay makes use of hypoxic incubation conditions to introduce DHE into the PM. A subsequent chase period under aerobic conditions enables DHE to redistribute to the ER where it is esterified, resulting in its eventual accumulation in LDs. Redistribution occurs presumably because DHE is displaced from the PM by ergosterol that is newly synthesized as oxygen becomes available. DHE redistribution is readily visualized by fluorescence microscopy; the cell cortex is stained at the start of the chase period, corresponding to DHE within the PM, whereas after 60 min fluorescence appears intracellularly, both diffusely throughout the cell and in the form of foci that co-label with LD markers. The ability to stop the redistribution process with energy poisons enabled us to obtain snapshots of transport and evaluate transport kinetics.

Our approaches to measure DHE redistribution detected a net unidirectional transport, from the PM to LDs, and from a free form to esters. Using this assay we tested the hypothesis that Osh proteins are required for intracellular sterol transport. Our experiments showed unambiguously that DHE moves from the PM to LDs in a temperature-sensitive strain (*osh*Δ *osh4-1*^{ts}) that lacks all functional Osh proteins at the non-permissive temperature, and that this redistribution is matched by its conversion to DHE esters. The time course of redistribution visualized by fluorescence microscopy and measured by HPLC analyses of ester formation revealed that it was only slightly slower in Osh-deficient cells compared with wild-type cells (Fig. 5C–E, G). Similar results were obtained via biochemical assays of cholesterol uptake (Figs. 5F, G). We consider the slight decrease in transport rate to be a downstream consequence of the loss of Osh protein function. Thus, we conclude that Osh proteins are dispensable for sterol transport from the PM to the ER and LDs.

We also measured the anterograde movement of ergosterol from the ER to the PM using pulse-chase labeling. To determine the amount of [^{3}H]ergosterol that had been transported to the PM we used subcellular fractionation to isolate a PM-enriched fraction devoid of major intracellular organelles (Fig. 6A). In a parallel analysis we isolated DRMs, a membrane fraction that is enriched in PM components (9, 42). Measurements of the delivery of pulse-labeled [^{3}H]ergosterol to the PM fraction and DRMs showed that anterograde movement of ergosterol is rapid ($t_{1/2} \leq 4$ min) in both wild-type and Osh-deficient cells (Figs. 6B, C). We could not refine the $t_{1/2}$ estimate further because of the time needed to generate an adequate pulse of radiolabeled ergosterol. We conclude that whereas Osh proteins may bind sterols and influence sterol homeostasis (36, 45, 46), their role in retrograde and anterograde sterol movement between the PM and ER is either minimal, or readily subsumed by other transport mechanisms that can handle the entire transport flux. Thus the molecular mechanism of the non-vesicular movement of yeast sterols remains to be determined.

Osh protein family members regulate the organization of sterols at the PM

We previously used MβCD sampling to monitor the delivery of [^{3}H]ergosterol to the PM in pulse-chase experiments(9). When this approach was employed to compare transport in wild-type and Osh-deficient cells (Fig. 7), the results were different from those obtained

with fractionation-based analyses of anterograde transport (Fig. 6C). First, delivery of [^{3}H]ergosterol to the PM in wild-type cells was much faster when assayed by fractionation than by MβCD extraction ($t_{1/2} \leq 4$ min vs ~20 min). Second, Osh-deficiency did not affect the transport rate as measured by fractionation methods, but slowed transport by an order of magnitude when measured by MβCD extraction. These apparently disparate results are reconciled in the model shown in Fig. 8.

We propose that PM sterol is organized in two pools, PM1 and PM2, as depicted in Fig. 8A. The essential features of this organization are: (i) newly synthesized ergosterol is delivered to PM1, (ii) MβCD extracts sterols solely from PM2, (iii) PM1 and PM2 are not distinguished in fractionation experiments and are co-isolated as a single PM or DRM fraction, and (iv) sterol can be exchanged between PM1 and PM2. With this model we propose that in wild-type cells, ergosterol is transported rapidly ($t_{1/2} \leq 4$) from the ER to PM1, then exchanges slowly ($t_{1/2}$ ~20 min) with PM2 (Fig. 8A). For Osh-deficient cells, transport of ergosterol from the ER to PM1 is as rapid as in wild-type cells, but exchange between PM1 and PM2 is much slower ($t_{1/2}$ ~200 min) (Fig. 8B).

What is the molecular nature of PM1 and PM2? The two pools may correspond to laterally or transversely segregated domains of sterol in the PM. For example, Tanner and colleagues report that sterols (visualized with filipin) are enriched in regions of the yeast PM defined by the arginine/H^+-symporter Can1, as well as by the eisosomal proteins Pil1 and Lsp1 (47–49), and that these regions are interspersed with areas in which sterol density is relatively low. This patchiness in sterol distribution may yield the two sterol populations suggested by our transport data. Another possibility that we consider to be more likely is that PM1 and PM2 correspond to ergosterol located in the inner and outer leaflet of the PM, respectively. This fits well with the assignment of PM1 as the site of STP-mediated ergosterol delivery through the cytoplasm and PM2 as the MβCD-accessible sterol pool. Sterol exchange between PM1 and PM2 would require transbilayer movement, normally considered to be a fast process ($t_{½} < 1$ min) based on measurements of sterol flip-flop across synthetic, liquid crystalline membranes and the membrane of red blood cells (43, 50, 51). However, the situation may be quite different for the yeast PM. The lateral diffusion of membrane components in the yeast PM is exceptionally slow (52, 53) and we speculate that the unassisted transbilayer movement of ergosterol in the yeast PM may also be far slower than predicted, accounting for the slow exchange ($t_{1/2}$ ~20 min) between PM1 and PM2 in wild-type cells (Fig. 8A). An additional point to note is the relative size of the two pools. This cannot be deduced from our data, but it is likely that sterols are distributed asymmetrically across the yeast PM, with the majority of the sterol molecules located in the cytoplasmic leaflet (D.P.S., A.G., A.K.M., unpublished observations) as suggested for the PM of mammalian cells (54). Thus the size of PM2 (outer leaflet sterol) is likely to be significantly smaller than that of PM1 (inner leaflet sterol) as depicted in Fig. 8A.

Our results indicate that the rate of sterol exchange between PM1 and PM2 is even lower in Osh-deficient cells than in wild-type cells. Although the reason(s) for this remain to be elucidated, it is clear that Osh proteins can influence the composition and organization of lipids at the PM. For example, phosphoinositide levels are elevated by an order of magnitude in Osh-deficient cells with phosphatidylinositol-4-phosphate specifically accumulating at the PM (55). Interestingly, *osh4*Δ cells display a partial loss of PM transbilayer phospholipid asymmetry due to the antagonistic interaction between Osh4 and the lipid flippase Drs2 (56). This change in phospholipid asymmetry may influence the transbilayer distribution of ergosterol in the PM and, in turn, the rate of ergosterol exchange between PM1 and PM2. Consistent with this notion is the finding that whereas ergosterol levels are unaffected in *osh4*Δ cells, these cells are very resistant to nystatin (20), a polyene anti-fungal compound that manifests toxicity by binding ergosterol on the PM surface.

The organization of PM sterol content into two, slowly exchanging pools is unlikely to impact our analyses of retrograde transport as (i) the yeast cells were labeled with DHE over a 36 hr period under hypoxic conditions, a sufficiently long time period to allow DHE to equilibrate fully with the PM, and (iii) the main source of DHE for esterification during the aerobic chase period would be PM1, as this is expected to be the larger of the two PM pools (see above), and (iii) the time resolution of this assay is poorer than that of the anterograde transport assays, with sterol esterification rather than PM-ER transport being the likely rate-limiting step.

We have proposed a model of sterol organization at the PM, and of ER-PM sterol movement, that accounts for all of the data. Built into the model is an unanticipated role for one or more Osh proteins in sorting and organizing sterols at the PM. Clearly, additional work is needed to define the molecular nature of the PM sterol pools and how Osh protein family members influence the rate of sterol exchange between them.

Yeast STPs?

A survey of the yeast proteome does not yield obvious STP candidates other than the Osh protein family that we have now eliminated from consideration. Mammalian Niemann-Pick Type C proteins 1 and 2 play a role in the egress of lipoprotein-derived cholesterol from lysosomes to the ER. Yeast cells express homologs of these proteins, Ncr1 and Npc2 (57, 58), but like their mammalian counterparts they are located in the vacuole membrane and the vacuolar lumen, respectively, and are unlikely to function in transport of ergosterol through the cytoplasm. It is possible that yeast STPs lack recognizable `lipid sequestering motifs' such as the StART domain and thus cannot be readily identified by bioinformatics approaches. For example, they may have intrinsically disordered domains (59) that could envelope a sterol for transit through the cytoplasm. Alternatively, sterol transfer between cellular compartments might occur at membrane contact sites through a mechanism that does not require STPs. Regardless of mechanism, proteins required for sterol transfer might be best identified through unbiased, genome-wide screens using an appropriate transport assay. The use of hypoxic conditions to introduce sterols into the yeast PM, followed by a chase period under aerobic conditions, provides a general method to establish a screen for transport mutants.

MATERIALS AND METHODS

Materials

Radiochemicals ([^{3}H-methyl]methionine (80 Ci/mmol), [4-^{14}C]cholesterol (50 mCi/mmol) and [1,2-^{3}H(N)]cholesterol (40 Ci/mmol)) were purchased from American Radiolabeled Chemicals. Methyl-β-cyclodextrin (MβCD), DHE (Ergosta-5,7,9(11),22-tetraen-3β-ol), cholesterol, ergosterol, 7-dehydrocholesterol, glass beads and Tween 80 were from Sigma Aldrich. Solvents were HPLC grade and purchased from Fisher Scientific or VWR International. Silica 60 thin layer chromatography plates were from Merck. Yeast media components were from Difco.

DHE was dissolved in absolute ethanol to 4 mg/mL. Equal volumes of DHE in ethanol and Tween 80 were mixed in a glass tube and the mixture was resuspended in growth media to achieve final concentrations of 0.5% (v/v) for ethanol and Tween 80, and 20 μg/mL DHE.

Hypoxic incubation

Yeast strains (Table 2) were inoculated from an overnight saturated liquid culture to OD_{600} ~0.05 in 10 mL culture tubes with 1 mL YPD supplemented with 20 μg/mL DHE, 0.5% ethanol, 0.5% Tween 80. The cultures, together with BD GasPak* EZ Anaerobe carbon

sachets (BD Diagnostics), were placed inside an anaerobe incubation chamber, the chamber was sealed and incubated for 36 hours at the appropriate temperature. The sachets reduce oxygen levels to 0.7% (v/v), yielding hypoxic conditions. To culture temperature-sensitive mutants at restrictive temperatures, anaerobe chambers were shifted to the appropriate temperature for one hour prior to further incubation for the desired duration; temperature inside the chamber was periodically monitored for accuracy. At the end of the hypoxic incubation, the chamber was opened, the culture removed and the media exchanged for fresh YPD containing 0.5% ethanol and Tween 80 and pre-equilibrated at the desired temperature. Subsequent incubation was done with continuous shaking.

Fluorescence microscopy

For microscopy, 50 μL samples were retrieved and diluted in 1 mL ice-cold 10 mM NaN_3, 10 mM NaF. The cells were kept on ice or incubated for 5 minutes at ambient temperature, stained with 2 μL Nile Red (1 mg/ml in acetone), and washed three times with ice-cold 10 mM NaN_3, 10 mM NaF. An 80 μL aliquot of the cell suspension was examined by fluorescence microscopy. Fluorescence microscopy and digital image acquisition were carried out using a Leica inverted microscope equipped with a Princeton Instruments cooled CCD camera driven by MetaMorph Imaging software. All images were acquired using a high magnification (63×, 1.4 NA) oil-immersion objective. DHE was imaged using a specially designed filter cube obtained from Chroma Technology (Brattleboro, VT, USA) with 335-nm (20-nm bandpass) excitation filter, 365-nm longpass dichromatic filter and 405-nm (40-nm bandpass) emission filter. Nile Red was imaged using a standard rhodamine filter set [535-nm (50-nm bandpass) excitation filter, 565-nm longpass dichromatic filter and 610-nm (75-nm bandpass) emission filter]. Images collected with the Metamorph software were subsequently processed with ImageJ for signal co-localization and quantification.

Quantification of DHE redistribution by analysis of fluorescence images

Two methods were used. *Manual scoring*. Cells with predominantly PM fluorescence were classified as “PM”, cells with punctate intracellular signal lacking a visible staining at the cell cortex were classified as “foci”, and cells with both PM and punctate signal or having only diffuse intracellular signal as “intermediate”. At least 200 cells were counted (from 4 to 12 individual viewing fields) for each strain, condition and discrete time-point. Standard deviation was calculated from the scores of at least three independent experiments performed on different days. *Automated scoring*. DIC images of the cells were used to define regions of the cell population directly corresponding to the periphery (PM) or the interior of cells using watershed thresholding. These regions were converted to masks and used to measure the fluorescence intensity captured by the corresponding DHE images. The remaining (cell-free) regions of the images were used for background correction. The fraction of cumulative intensity for the cell interior after background subtraction was used as a measure for DHE redistribution from the PM to the cell interior.

Lipid extraction from post-hypoxically grown cells

Following hypoxic incubation, cultures were incubated aerobically for an additional 60 minutes. Samples of 1 mL were collected at regular intervals (0, 20, 40 and 60 min) and added to 1 mL ice-cold 10 mM NaN_3, 10 mM NaF. After 5 minutes on ice, the samples were centrifuged, washed two more times, and resuspended in 200 μL azide/fluoride solution. Glass beads were added and the cells were disrupted by 6× rigorous vortexing for 45 sec interrupted by 45 seconds chilling on ice. The liquid volume was adjusted to 1 mL, the cell lysate was recovered in glass sample tubes and the non-polar lipids extracted with hexane.

HPLC and TLC analysis of lipids

Ergosterol and DHE were separated from their corresponding esterified forms by reversed phase-HPLC on a C18 spherisorb column (S5 ODS2, 4.6×250 mm) (Waters, Milford, MA) (60). Sterol-containing lipid extracts dissolved in 100 μL acetonitrile were manually injected using a 200 μL injection loop, eluted with acetonitrile/isopropanol (50:50, 1 mL/min), detected at 280 nm (ergosterol) or 325 nm (DHE) using a Waters 2487 detector, and quantified using a Waters 746 data module integrator. Detector response to both sterols was calibrated, and measurements were carried out in a linear response range.

Cholesterol and cholesteryl esters were resolved on silica 60 thin layer plates with hexane:diethylether:acetic acid (70:30:1, by volume) as the solvent system. [^{14}C]-chromatograms were visualized by autoradiography and quantified with ImageJ; [^{3}H]-labeled samples were visualized and quantified using a Berthold LB2842 TLC scanner.

ACAT assay

Acyl-CoA:sterol acyltransferase activity was assayed *in vitro* using a modification of a published procedure (61). Microsomes were prepared from yeast cell cultures that had been incubated under hypoxic conditions for 36 hrs at RT (OD_{600} 3–5), incubated for 1 hr at 37°C and incubated aerobically for 30 minutes at 37°C. After chilling on ice the cells were washed with cold sterile water, resuspended in Reaction Buffer (RB, 0.1 M potassium phosphate, pH 7.4, 1 mM reduced glutathione), and vortexed with glass beads to generate a cell homogenate. The homogenate was centrifuged at 1000 × g for 3 min to remove unbroken cells before being further centrifuged for 1 hr at 100,000 × g at 4°C to pellet microsomes. The microsomal pellet was resuspended in RB using a small glass pestle. Microsome protein concentration was measured by the micro-BCA method.

Sterols (taken from organic solvent stocks) were dried in glass tubes and resuspended in RB containing 10 mM MβCD to a final concentration of 1 mM ([^{3}H]cholesterol) or 200 μM (DHE). The *in vitro* reaction mix containing 200 μL microsomes, 100 nmol sterol, and 1 mg of defatted bovine serum albumin in a total volume of 800 μL of RB, was pre-incubated for 15 min at 30°C, after which it was cooled to ambient temperature. The ACAT reaction was started by adding 20 nmol oleoyl-CoA (from a 4.8 mM stock). Aliquots of 250 μL of the reaction were withdrawn at 10 min intervals starting directly after the addition of the oleoyl-CoA, and mixed with 2 mL hexane/isopropanol for lipid extraction. Unreacted sterols and steryl oleate were estimated by TLC ([^{3}H]cholesterol) or HPLC (DHE) as described above. ACAT activity (linear for at least 30 min) was calculated as moles sterol esterified per μg protein per minute.

MβCD sampling to measure transport of ergosterol from the ER to the PM

Overnight cultures (50 ml at OD_{600}~3.0) were diluted to OD600 1.5 and allowed to double at room temperature (~2 hrs). The cultures were then incubated for 90 min at 37°C to induce the temperature sensitive phenotype of the *osh*Δ *osh4-1^{ts}* strain. Pulse-chase labeling with [^{3}H-methyl]methionine, MβCD extraction and lipid analysis were carried out exactly as previously described (9). The specific radioactivity of [^{3}H]ergosterol in the MβCD extract was normalized to that in whole cells to obtain a `relative specific radioactivity' or RSR.

Sucrose gradient fractionation assay to measure transport of ergosterol from the ER to the PM

Cell cultures were prepared exactly as described for the MβCD sampling assay. 5 mL aliquots were retrieved from the culture at the end of the pulse labeling period and after a 90 min chase and added to 20 mL of cold 20 mM sodium azide on ice. The samples were further washed three times with cold 10 mM azide and resuspended in Breaking Buffer (BB;

10 mM azide, 10 mM HEPES pH 7.2 and 1 mM EDTA). 100 OD equivalents of cells were resuspended in 300 μL of BB, 300 μL glass beads were added to the suspension and the cells were lysed by a 5 minute continuous vortexing at high speed in the cold. The suspension was diluted to 1 mL, transferred to a new tube, and centrifuged twice at 1000 × *g* to remove cell debris.

The cell lysate was analyzed by sucrose gradient fractionation (37, 38). The gradient was prepared in gradient buffer (10 mM HEPES-KOH, pH 7.2, 1 mM EDTA, 0.8 M sorbitol) using the following steps: 0.2 ml 60%, 0.4 ml 40%, 0.4 ml 37%, 0.6 ml 34%, 1 ml 32%, 1 ml 29%, 0.6 ml 27%, and 0.6 ml 22% (wt/wt) sucrose. The cell lysate (500 μL) was loaded on top of the gradient and centrifuged at 45,000 rpm in a Beckman MLS50 rotor (16 h, 4°C). Fractions (14 × 360-μL) were collected from the top.

Neutral lipids were isolated from 250 μL of the fractions pooled pairwise, added to 500 μL distilled water, and extracted with hexane/isopropanol as described above. Samples to be analyzed by immunoblotting were initially diluted 10 fold with 10 mM HEPES-KOH, pH 7.2, 1 mM EDTA, and membranes were collected by ultracentrifugation at 100,000 × g for 45 minutes. The membrane pellets were dissolved in 30μL sample buffer, proteins separated by SDS-PAGE and electroblotted onto PVDF membrane. Antibodies for immunoblot analysis were directed against Dpm1 and Pep12 (both from Molecular Probes), Sec61 (from Tom Rapoport, Harvard Medical School), Gas1 (from Andreas Conzelmann, University of Fribourg), Vph1 (from Patricia Kane, SUNY Upstate Medical University), and Mnn1 (from Todd Graham, Vanderbilt University).

DRMs

DRMs were isolated as described previously (9).

Acknowledgments

We thank Roger Schneiter, Wylie Nichols, Chris Stefan and Scott Emr for providing plasmids and strains, Andreas Conzelmann, Todd Graham, Patty Kane and Tom Rapoport for antibodies, Fred Maxfield for use of a fluorescence microscope, John Silvius for helpful discussions, Henna Ohvo-Rekilä for contributing to initial studies of ergosterol transport in Osh-deficient cells, and Bruno Mesmin for comments on the manuscript. Bob Dylan is acknowledged for seventy reasons. This work was supported by the NIH (grants GM55427 (A.K.M.) and GM095674 (J.S.D.)), the American Heart Association (postdoctoral fellowship to M.C.K.) and NSERC (C.T.B.).

REFERENCES

1. Maxfield FR, van Meer G. Cholesterol, the central lipid of mammalian cells. Curr Opin Cell Biol. 2010; 22(4):422–429. [PubMed: 20627678]
2. Liscum L, Munn NJ. Intracellular cholesterol transport. Biochim Biophys Acta. 1999; 1438(1):19–37. [PubMed: 10216277]
3. Maxfield FR, Wustner D. Intracellular cholesterol transport. J Clin Invest. 2002; 110(7):891–898. [PubMed: 12370264]
4. Maxfield FR, Menon AK. Intracellular sterol transport and distribution. Curr Opin Cell Biol. 2006; 18(4):379–385. [PubMed: 16806879]
5. Mesmin B, Maxfield FR. Intracellular sterol dynamics. Biochim Biophys Acta. 2009; 1791(7):636–645. [PubMed: 19286471]
6. Sullivan DP, Ohvo-Rekila H, Baumann NA, Beh CT, Menon AK. Sterol trafficking between the endoplasmic reticulum and plasma membrane in yeast. Biochem Soc Trans. 2006; 34(Pt 3):356–358. [PubMed: 16709160]
7. Zinser E, Paltauf F, Daum G. Sterol composition of yeast organelle membranes and subcellular distribution of enzymes involved in sterol metabolism. J Bacteriol. 1993; 175(10):2853–2858. [PubMed: 8491706]

8. Schneiter R, Brugger B, Sandhoff R, Zellnig G, Leber A, Lampl M, Athenstaedt K, Hrastnik C, Eder S, Daum G, Paltauf F, Wieland FT, Kohlwein SD. Electrospray ionization tandem mass spectrometry (ESI-MS/MS) analysis of the lipid molecular species composition of yeast subcellular membranes reveals acyl chain-based sorting/remodeling of distinct molecular species en route to the plasma membrane. J Cell Biol. 1999; 146(4):741–754. [PubMed: 10459010]
9. Baumann NA, Sullivan DP, Ohvo-Rekila H, Simonot C, Pottekat A, Klaassen Z, Beh CT, Menon AK. Transport of newly synthesized sterol to the sterolenriched plasma membrane occurs via nonvesicular equilibration. Biochemistry. 2005; 44(15):5816–5826. [PubMed: 15823040]
10. Schnabl M, Daum G, Pichler H. Multiple lipid transport pathways to the plasma membrane in yeast. Biochim Biophys Acta. 2005; 1687(1–3):130–140. [PubMed: 15708361]
11. Li Y, Prinz WA. ATP-binding cassette (ABC) transporters mediate nonvesicular, raft-modulated sterol movement from the plasma membrane to the endoplasmic reticulum. J Biol Chem. 2004; 279(43):45226–45234. [PubMed: 15316012]
12. Mullner H, Daum G. Dynamics of neutral lipid storage in yeast. Acta Biochim Pol. 2004; 51(2): 323–347. [PubMed: 15218532]
13. Jacquier N, Schneiter R. Mechanisms of sterol uptake and transport in yeast. J Steroid Biochem Mol Biol. 2010
14. Hanada K, Kumagai K, Tomishige N, Yamaji T. CERT-mediated trafficking of ceramide. Biochim Biophys Acta. 2009; 1791(7):684–691. [PubMed: 19416656]
15. Alpy F, Tomasetto C. Give lipids a START: the StAR-related lipid transfer (START) domain in mammals. J Cell Sci. 2005; 118(Pt 13):2791–2801. [PubMed: 15976441]
16. Strauss JF 3rd, Kishida T, Christenson LK, Fujimoto T, Hiroi H. START domain proteins and the intracellular trafficking of cholesterol in steroidogenic cells. Mol Cell Endocrinol. 2003; 202(1–2): 59–65. [PubMed: 12770731]
17. Schulz TA, Prinz WA. Sterol transport in yeast and the oxysterol binding protein homologue (OSH) family. Biochim Biophys Acta. 2007; 1771(6):769–780. [PubMed: 17434796]
18. Raychaudhuri S, Im YJ, Hurley JH, Prinz WA. Nonvesicular sterol movement from plasma membrane to ER requires oxysterol-binding protein-related proteins and phosphoinositides. J Cell Biol. 2006; 173(1):107–119. [PubMed: 16585271]
19. Im YJ, Raychaudhuri S, Prinz WA, Hurley JH. Structural mechanism for sterol sensing and transport by OSBP-related proteins. Nature. 2005; 437(7055):154–158. [PubMed: 16136145]
20. Beh CT, Cool L, Phillips J, Rine J. Overlapping functions of the yeast oxysterol-binding protein homologues. Genetics. 2001; 157(3):1117–1140. [PubMed: 11238399]
21. Schulz TA, Choi MG, Raychaudhuri S, Mears JA, Ghirlando R, Hinshaw JE, Prinz WA. Lipid-regulated sterol transfer between closely apposed membranes by oxysterol-binding protein homologues. J Cell Biol. 2009; 187(6):889–903. [PubMed: 20008566]
22. Woods RA, Bard M, Gardner IE, Molzahn SW. Studies on the accumulation of ergosterol and 24(28)-dehydroergosterol in 3 strains of *Saccharomyces cerevisiae*. Microbios. 1974; 10A(SUPPL(41)):73–80. [PubMed: 4617129]
23. Wustner D. Fluorescent sterols as tools in membrane biophysics and cell biology. Chem Phys Lipids. 2007; 146(1):1–25. [PubMed: 17241621]
24. Gollub EG, Liu KP, Dayan J, Adlersberg M, Sprinson DB. Yeast mutants deficient in heme biosynthesis and a heme mutant additionally blocked in cyclization of 2,3-oxidosqualene. J Biol Chem. 1977; 252(9):2846–2854. [PubMed: 323256]
25. Bard M. Biochemical and genetic aspects of nystatin resistance in *Saccharomyces cerevisiae*. J Bacteriol. 1972; 111(3):649–657. [PubMed: 4559817]
26. Kohut P, Wustner D, Hronska L, Kuchler K, Hapala I, Valachovic M. The role of ABC proteins Aus1p and Pdr11p in the uptake of external sterols in yeast: dehydroergosterol fluorescence study. Biochem Biophys Res Commun. 2011; 404(1):233–238. [PubMed: 21110944]
27. Keesler GA, Casey WM, Parks LW. Stimulation by heme of steryl ester synthase and aerobic sterol exclusion in the yeast *Saccharomyces cerevisiae*. Arch Biochem Biophys. 1992; 296(2): 474–481. [PubMed: 1632640]
28. Parks LW, Casey WM. Physiological implications of sterol biosynthesis in yeast. Annu Rev Microbiol. 1995; 49:95–116. [PubMed: 8561481]

29. Wilcox LJ, Balderes DA, Wharton B, Tinkelenberg AH, Rao G, Sturley SL. Transcriptional profiling identifies two members of the ATP-binding cassette transporter superfamily required for sterol uptake in yeast. J Biol Chem. 2002; 277(36):32466–32472. [PubMed: 12077145]
30. Chang A. Plasma membrane biogenesis. Methods Enzymol. 2002; 351:339–350. [PubMed: 12073354]
31. Yu C, Kennedy NJ, Chang CC, Rothblatt JA. Molecular cloning and characterization of two isoforms of *Saccharomyces cerevisiae* acyl-CoA:sterol acyltransferase. J Biol Chem. 1996; 271(39):24157–24163. [PubMed: 8798656]
32. Valachovic M, Hronska L, Hapala I. Anaerobiosis induces complex changes in sterol esterification pattern in the yeast *Saccharomyces cerevisiae*. FEMS Microbiol Lett. 2001; 197(1):41–45. [PubMed: 11287144]
33. Klein HP. Synthesis of lipids in resting cells of *Saccharomyces cerevisiae*. J Bacteriol. 1955; 69(6):620–627. [PubMed: 14392117]
34. Raths S, Rohrer J, Crausaz F, Riezman H. end3 and end4: two mutants defective in receptor-mediated and fluid-phase endocytosis in *Saccharomyces cerevisiae*. J Cell Biol. 1993; 120(1):55–65. [PubMed: 8380177]
35. Vida TA, Emr SD. A new vital stain for visualizing vacuolar membrane dynamics and endocytosis in yeast. J Cell Biol. 1995; 128(5):779–792. [PubMed: 7533169]
36. Beh CT, Rine J. A role for yeast oxysterol-binding protein homologs in endocytosis and in the maintenance of intracellular sterol-lipid distribution. J Cell Sci. 2004; 117(Pt 14):2983–2996. [PubMed: 15173322]
37. De Craene JO, Coleman J, Estrada de Martin P, Pypaert M, Anderson S, Yates JR 3rd, Ferro-Novick S, Novick P. Rtn1p is involved in structuring the cortical endoplasmic reticulum. Mol Biol Cell. 2006; 17(7):3009–3020. [PubMed: 16624861]
38. Pomorski T, Lombardi R, Riezman H, Devaux PF, van Meer G, Holthuis JC. Drs2p-related P-type ATPases Dnf1p and Dnf2p are required for phospholipid translocation across the yeast plasma membrane and serve a role in endocytosis. Mol Biol Cell. 2003; 14(3):1240–1254. [PubMed: 12631737]
39. Kaplan MR, Simoni RD. Transport of cholesterol from the endoplasmic reticulum to the plasma membrane. J Cell Biol. 1985; 101(2):446–453. [PubMed: 4040520]
40. Estronca LM, Moreno MJ, Vaz WL. Kinetics and thermodynamics of the association of dehydroergosterol with lipid bilayer membranes. Biophys J. 2007; 93(12):4244–4253. [PubMed: 17766353]
41. Silvius JR, Leventis R. Spontaneous interbilayer transfer of phospholipids: dependence on acyl chain composition. Biochemistry. 1993; 32(48):13318–13326. [PubMed: 8241188]
42. Bagnat M, Keranen S, Shevchenko A, Simons K. Lipid rafts function in biosynthetic delivery of proteins to the cell surface in yeast. Proc Natl Acad Sci U S A. 2000; 97(7):3254–3259. [PubMed: 10716729]
43. John K, Kubelt J, Muller P, Wustner D, Herrmann A. Rapid transbilayer movement of the fluorescent sterol dehydroergosterol in lipid membranes. Biophys J. 2002; 83(3):1525–1534. [PubMed: 12202377]
44. Sullivan DP, Georgiev A, Menon AK. Tritium suicide selection identifies proteins involved in the uptake and intracellular transport of sterols in Saccharomyces cerevisiae. Eukaryot Cell. 2008
45. Fairn GD, McMaster CR. Emerging roles of the oxysterol-binding protein family in metabolism, transport, and signaling. Cell Mol Life Sci. 2008; 65(2):228–236. [PubMed: 17938859]
46. Raychaudhuri S, Prinz WA. The Diverse Functions of Oxysterol-Binding Proteins. Annu Rev Cell Dev Biol. 2010
47. Grossmann G, Opekarova M, Malinsky J, Weig-Meckl I, Tanner W. Membrane potential governs lateral segregation of plasma membrane proteins and lipids in yeast. EMBO J. 2007; 26(1):1–8. [PubMed: 17170709]
48. Grossmann G, Malinsky J, Stahlschmidt W, Loibl M, Weig-Meckl I, Frommer WB, Opekarova M, Tanner W. Plasma membrane microdomains regulate turnover of transport proteins in yeast. J Cell Biol. 2008; 183(6):1075–1088. [PubMed: 19064668]

49. Malinsky J, Opekarova M, Tanner W. The lateral compartmentation of the yeast plasma membrane. Yeast. 2010; 27(8):473–478. [PubMed: 20641012]
50. Leventis R, Silvius JR. Use of cyclodextrins to monitor transbilayer movement and differential lipid affinities of cholesterol. Biophys J. 2001; 81(4):2257–2267. [PubMed: 11566796]
51. Steck TL, Ye J, Lange Y. Probing red cell membrane cholesterol movement with cyclodextrin. Biophys J. 2002; 83(4):2118–2125. [PubMed: 12324429]
52. Greenberg ML, Axelrod D. Anomalously slow mobility of fluorescent lipid probes in the plasma membrane of the yeast Saccharomyces cerevisiae. J Membr Biol. 1993; 131(2):115–127. [PubMed: 8441175]
53. Valdez-Taubas J, Pelham HR. Slow diffusion of proteins in the yeast plasma membrane allows polarity to be maintained by endocytic cycling. Curr Biol. 2003; 13(18):1636–1640. [PubMed: 13678596]
54. Mondal M, Mesmin B, Mukherjee S, Maxfield FR. Sterols are mainly in the cytoplasmic leaflet of the plasma membrane and the endocytic recycling compartment in CHO cells. Mol Biol Cell. 2009; 20(2):581–588. [PubMed: 19019985]
55. Stefan CJ, Manford AG, Baird D, Yamada-Hanff J, Mao Y, Emr SD. Osh proteins regulate phosphoinositide metabolism at ER-plasma membrane contact sites. Cell. 2011; 144(3):389–401. [PubMed: 21295699]
56. Muthusamy BP, Raychaudhuri S, Natarajan P, Abe F, Liu K, Prinz WA, Graham TR. Control of protein and sterol trafficking by antagonistic activities of a type IV P-type ATPase and oxysterol binding protein homologue. Mol Biol Cell. 2009; 20(12):2920–2931. [PubMed: 19403696]
57. Berger AC, Vanderford TH, Gernert KM, Nichols JW, Faundez V, Corbett AH. Saccharomyces cerevisiae Npc2p is a functionally conserved homologue of the human Niemann-Pick disease type C 2 protein, hNPC2. Eukaryot Cell. 2005; 4(11):1851–1862. [PubMed: 16278452]
58. Berger AC, Hanson PK, Wylie Nichols J, Corbett AH. A yeast model system for functional analysis of the Niemann-Pick type C protein 1 homolog, Ncr1p. Traffic. 2005; 6(10):907–917. [PubMed: 16138904]
59. Eliezer D. Biophysical characterization of intrinsically disordered proteins. Curr Opin Struct Biol. 2009; 19(1):23–30. [PubMed: 19162471]
60. Rodriguez RJ, Parks LW. High-performance liquid chromatography of sterols: yeast sterols. Methods Enzymol. 1985; 111:37–51. [PubMed: 3897778]
61. Billheimer JT, Tavani D, Nes WR. Effect of a dispersion of cholesterol in Triton WR-1339 on acyl CoA: cholesterol acyltransferase in rat liver microsomes. Anal Biochem. 1981; 111(2):331–335. [PubMed: 7247027]
62. Nuoffer C, Jeno P, Conzelmann A, Riezman H. Determinants for glycophospholipid anchoring of the Saccharomyces cerevisiae GAS1 protein to the plasma membrane. Mol Cell Biol. 1991; 11(1): 27–37. [PubMed: 1824714]
63. Deshaies RJ, Schekman R. A yeast mutant defective at an early stage in import of secretory protein precursors into the endoplasmic reticulum. J Cell Biol. 1987; 105(2):633–645. [PubMed: 3305520]
64. Manolson MF, Proteau D, Preston RA, Stenbit A, Roberts BT, Hoyt MA, Preuss D, Mulholland J, Botstein D, Jones EW. The VPH1 gene encodes a 95-kDa integral membrane polypeptide required for in vivo assembly and activity of the yeast vacuolar H(+)-ATPase. J Biol Chem. 1992; 267(20): 14294–14303. [PubMed: 1385813]
65. Becherer KA, Rieder SE, Emr SD, Jones EW. Novel syntaxin homologue, Pep12p, required for the sorting of lumenal hydrolases to the lysosome-like vacuole in yeast. Mol Biol Cell. 1996; 7(4): 579–594. [PubMed: 8730101]
66. Graham TR, Seeger M, Payne GS, MacKay VL, Emr SD. Clathrin-dependent localization of alpha 1,3 mannosyltransferase to the Golgi complex of Saccharomyces cerevisiae. J Cell Biol. 1994; 127(3):667–678. [PubMed: 7962051]
67. Robinson JS, Klionsky DJ, Banta LM, Emr SD. Protein sorting in Saccharomyces cerevisiae: isolation of mutants defective in the delivery and processing of multiple vacuolar hydrolases. Mol Cell Biol. 1988; 8(11):4936–4948. [PubMed: 3062374]

68. Koffel R, Schneiter R. Yeh1 constitutes the major steryl ester hydrolase under heme-deficient conditions in Saccharomyces cerevisiae. Eukaryot Cell. 2006; 5(7):1018–1025. [PubMed: 16835446]

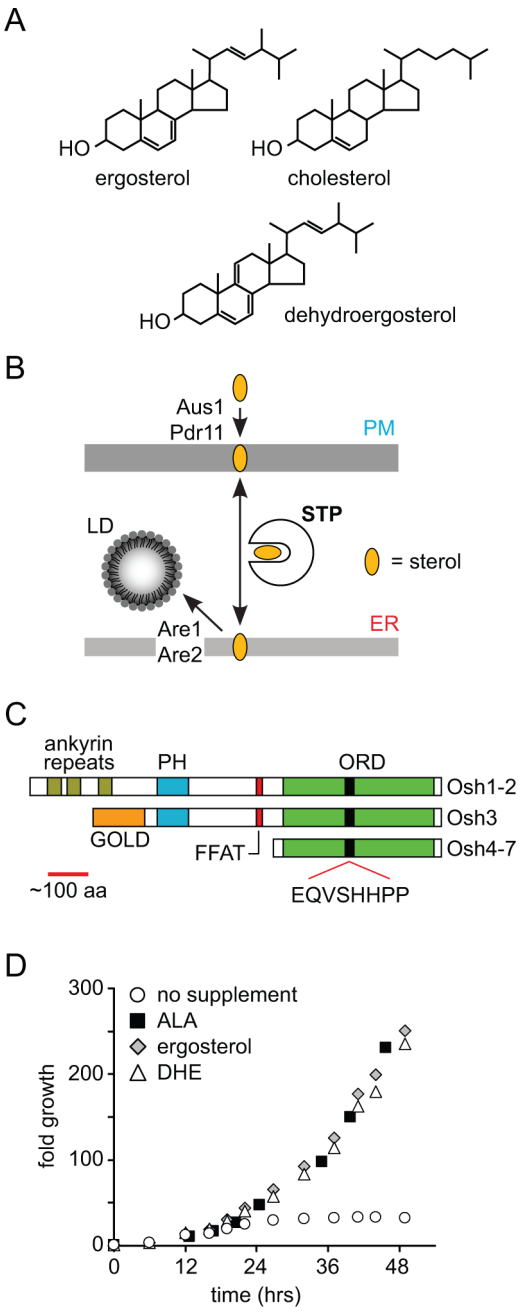

Figure 1. Intracellular sterol transport and Osh proteins

A. Chemical structures of sterols.

B. Non-vesicular intracellular sterol pathways. Under normal aerobic growth conditions, sterols are synthesized in the endoplasmic reticulum (ER) and transported bi-directionally between the ER and the plasma membrane (PM), presumably by one or more sterol transport proteins (STPs). For anaerobically or hypoxically grown cells, sterols must be provided in the extracellular medium. They enter the PM as a result of the activity of the ABC transporters Aus1 and Pdr11 that are expressed solely under hypoxic/anaerobic conditions. STP-mediated transport to the ER results in esterification and storage of the resulting steryl esters in lipid droplets (LDs). Esterification is catalyzed by the ER-localized acyl transferases Are1 and Are2.

C. Schematic representation of the domain structure of the family of yeast oxysterol binding protein homologues (Osh1–7). GOLD, Golgi dynamics; PH, pleckstrin homology; FFAT, two phenylalanines in an acidic tract; ORD, oxysterol binding protein-related domain containing the signature motif EQVSHHPP.
D. Growth of *hem1*Δ (YRS1707) cells in synthetic media containing 0.5% (w/v) Tween 80, 0.5% (v/v) ethanol and no supplement, 10 μg/ml aminolevulinic acid (ALA), 20 μg/ml ergosterol (ERG), or 20 μg/ml dehydroergosterol (DHE) as indicated.

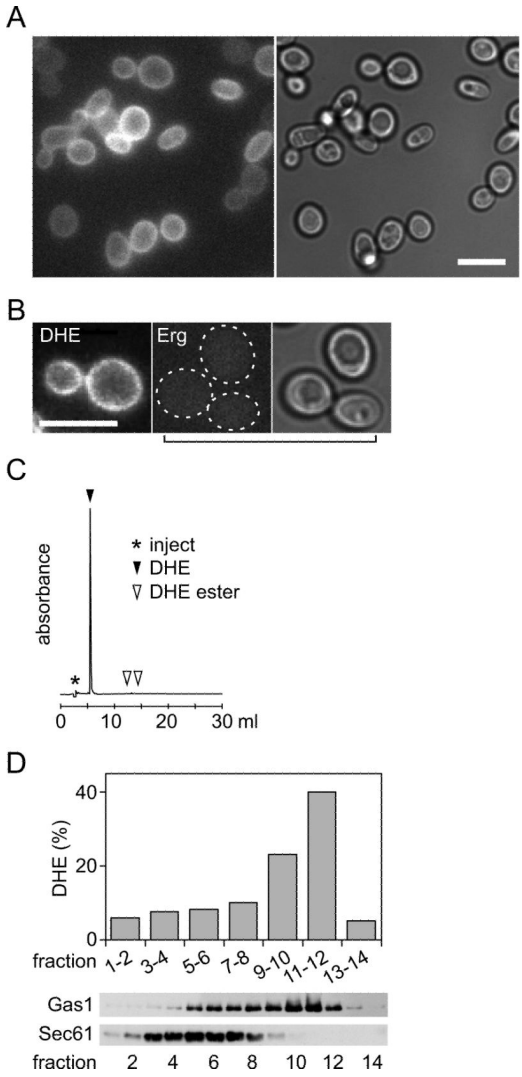

Figure 2. Incorporation of DHE into the PM of cells grown under hypoxic conditions

A. Epifluorescence and DIC images of wild-type (SEY6210) yeast cells grown under hypoxic conditions (<0.7% O_2) for 40 hr in YPD supplemented with 20 μg/mL DHE in 0.5% ethanol, 0.5% Tween 80; scale bar 20 μm.

B. Comparison of cells grown under hypoxic conditions in YPD supplemented with DHE (left) or ergosterol (Erg, two right panels); the two left panels show epifluorescence images whereas the right panel shows a DIC image corresponding to the middle panel; scale bar 20 μm.

C. Reversed phase HPLC analysis of DHE extracted from cells obtained as in panel A.

D. A homogenate of DHE-loaded cells was fractionated on a Renocal gradient. Gradient fractions were analyzed by SDS-PAGE immunoblotting with organelle-specific antibodies (PM, anti-Gas1; ER, anti-Sec61) and also subjected to lipid extraction and HPLC analysis to determine their DHE content (% of total).

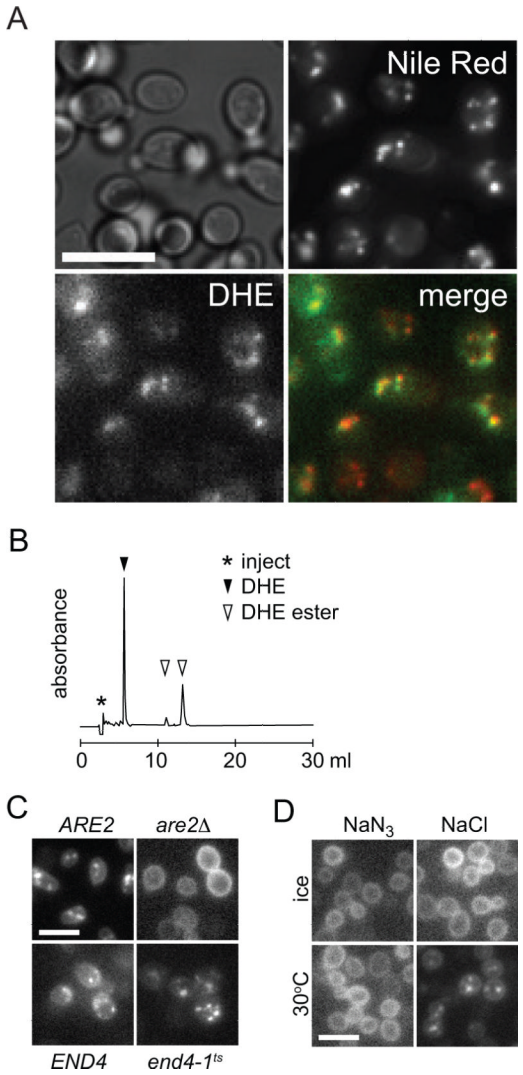

Figure 3. Redistribution of DHE from the PM to lipid droplets

A. Images of wild-type (SEY6210) cells loaded hypoxically with DHE and subsequently grown aerobically for 60 min. The cells were stained with Nile Red at the end of the aerobic incubation. DIC, DHE and Nile Red images are shown. A merge of the latter images is shown at bottom right (green, DHE; red, Nile Red). Scale bar 20 μm.

B. Reversed phase HPLC analysis of DHE extracted from cells obtained as in panel A.

C. Yeast strains as indicated were loaded hypoxically with DHE and subsequently grown aerobically for 60 min before imaging, either at 30°C (*ARE2* (BY4741) and *are2*Δ) or at 37°C (*END4* (RH448) and *end4-1*^{ts} (RH1597)).

D. Wild-type (SEY6210) cells were loaded hypoxically with DHE and subsequently incubated aerobically for 60 min on ice or at 30°C in the presence (NaN_3) or absence (NaCl) of energy poison.

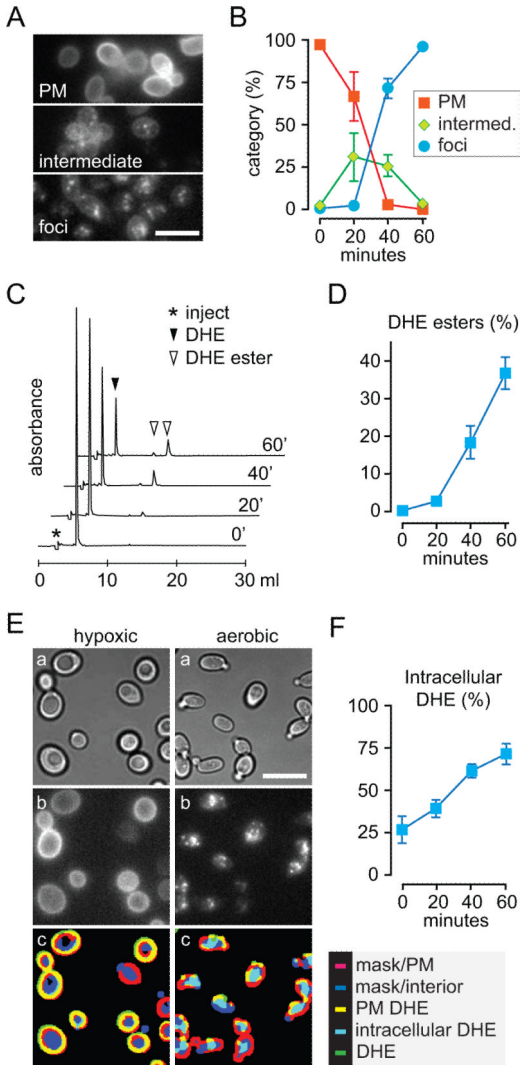

Figure 4. Quantification of DHE redistribution from the PM to LDs

A. Fluorescence patterns used to categorize cells.

B. Wild-type (SEY6210) cells were loaded with DHE under hypoxic conditions then incubated aerobically for 0–60 min. Fluorescence images were acquired at each time point and manually scored by assigning individual cells to the categories illustrated in panel A. Data are from three independent experiments; at least 200 cells were counted for each time point in each experiment. Scale bar 20 μm.

C. DHE loaded wild-type (SEY6210) cells were processed as in panel B except that at each time point an aliquot of the cells was taken for lipid extraction and HPLC analysis to resolve and quantify DHE and DHE esters. The figure shows stacked HPLC profiles of individual analyses corresponding to different time points.

D. Data from 3 independent analyses similar to those shown in C were quantified to determine the percentage of DHE that was converted to ester during the aerobic incubation period.

E. Example of image processing used to quantify intracellular DHE fluorescence. The left column shows images of cells loaded with DHE under hypoxic conditions, the right column the same cell culture after 60 min aerobic incubation. DIC images (a) are used to define

masks for cell rim and interior, and these masks are merged with enhanced DHE epi-fluorescence (b) to illustrate DHE localization (c). Scale bar 20 μm.
F. Data from 3 independent analyses similar to those shown in panel E were quantified to determine the percentage of intracellular DHE at different times during the aerobic incubation period.

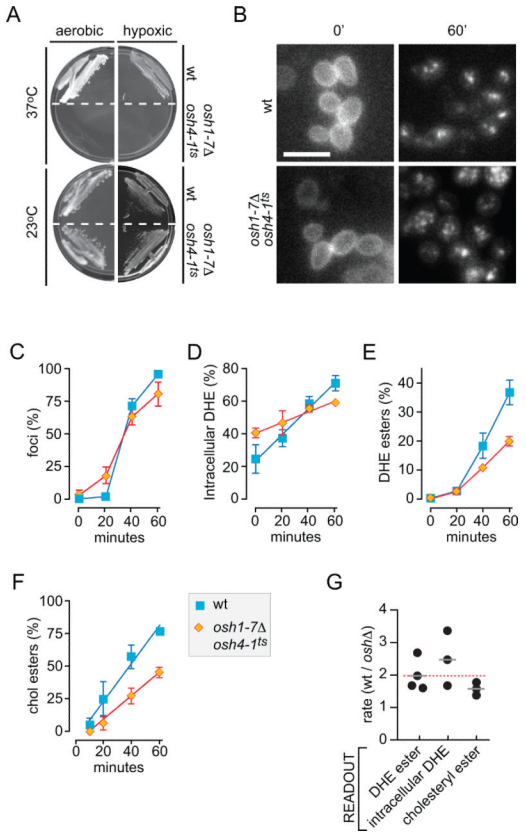

Figure 5. DHE redistribution from the PM to LDs in cells lacking functional Osh proteins

A. A mutant strain (CBY926) lacking all 7 *OSH* genes and supported by a temperature-sensitive *osh4-1*^{ts} allele fails to grow at the restrictive temperature of 37°C both under aerobic and hypoxic conditions.

B. Aerobic redistribution of DHE in *osh*Δ *osh4-1*^{ts} cells. Cells were cultured hypoxically at 23°C in the presence of DHE, then incubated at 37°C for 1 hr before transfer to aerobic conditions for 0 or 60 min. Wild-type cells were analyzed in parallel. Scale bar = 20 μm.

C. Quantification of DHE redistribution time-course in *osh*Δ *osh4-1*^{ts} (diamonds) and wild-type (squares) cells by manual scoring.

D. Quantification of DHE redistribution time-course in *osh*Δ *osh4-1*^{ts} (diamonds) and wild-type (squares) cells by automated image analysis.

E. Quantification of DHE redistribution time-course in *osh*Δ *osh4-1*^{ts} (diamonds) and wild-type (squares) cells by HPLC measurement of DHE estrs.

F. [^{14}C]Cholesterol uptake and esterification in wild-type and *osh*Δ *osh4-1*^{ts} cells that were pre-grown under hypoxic conditions, incubated at 37°C for 1 hr and then supplied with labeled cholesterol during aerobic incubation for 0–60 min at 37°C. The graph shows quantification of cholesterol esterification data compiled from 3 independent experiments. The fraction of cholesteryl esters is normalized to total cellular radiolabeled sterols at 60 min to allow for comparison with DHE esterification data.

G. Ratio of the rate of sterol redistribution from the PM to intracellular compartments in wild-type cells versus *osh*Δ *osh4-1*^{ts} cells at 37°C. Individual experiments are shown, using three different experimental readouts. The average value for each type of measurement is indicated (grey bar.) The red dotted line is the average of all ten analyses.

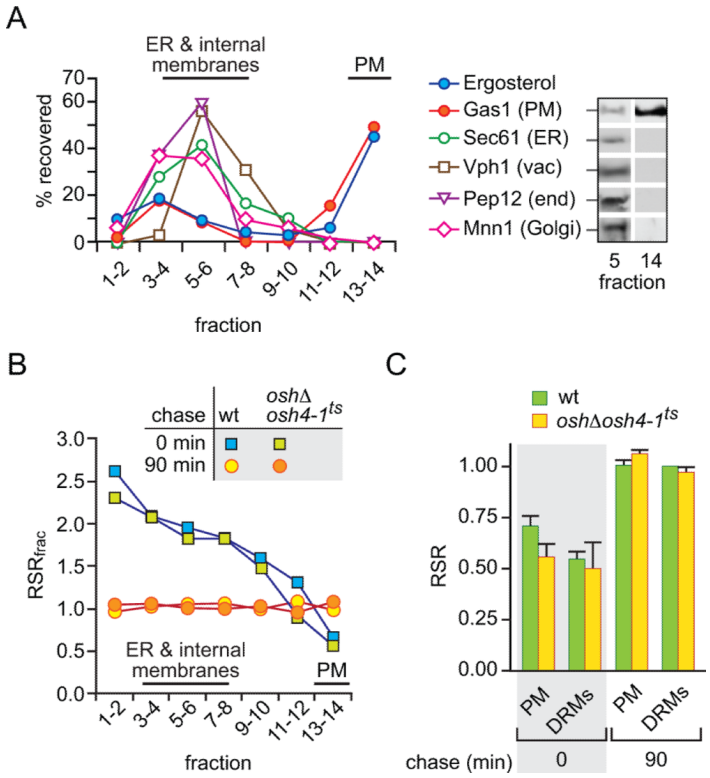

Figure 6. Delivery of newly synthesized ergosterol from the ER to the PM assayed by sub-cellular fractionation

A. Analysis of sucrose gradient fractions by ergosterol analysis and immunoblotting using antibodies against Gas1 (PM)(62), Sec61 (ER)(63), Vph1 (vacuole)(64), Pep12 (endosome)(65) and Mnn1 (Golgi)(66). Immunoblots were quantitated by densitometry and graphed as the percentage of total signal recovered in fractions taken pair wise from the top of the gradient. Individual blots for fractions 5 and 14 are shown at the right. The data correspond to *oshΔ osh4-1*^{ts} cells at the end of the 90 min chase period; similar profiles were obtained for wild-type cells and end-of-pulse samples.

B. Wild-type (wt) and *oshΔ osh4-1*^{ts} cells were pulse-labeled and chased for 90 min at 37°C. Samples taken at the end of the pulse labeling period (chase = 0 min) and at the end of the chase (chase = 90 min) were fractionated on sucrose gradients. The specific radioactivity (SR = cpm ÷ absorbance units) of ergosterol was determined for subcellular fractions as well as for whole cells by HPLC analysis, and the relative specific radioactivity ($RSR_{frac} = SR_{frac} \div SR_{cell}$) of fractions pooled pairwise from the top of the gradient was calculated. See Results and Materials and Methods for experimental details.

C. Wild-type (wt) and *oshΔ osh4-1*^{ts} cells were pulse-labeled and chased for 90 min at 37°C. Samples were taken at the end of the pulse labeling period (chase time = 0 min) and after the chase (90 min) to isolate PM and DRMs. The bar chart shows the RSR of [^{3}H]ergosterol in the PM-enriched fraction and DRMs.

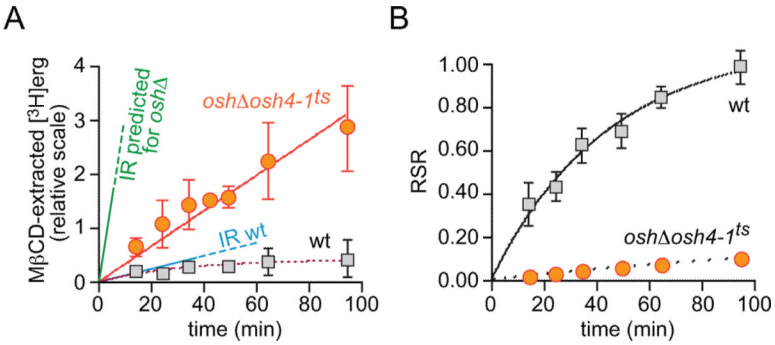

Figure 7. Delivery of newly synthesized ergosterol from the ER to the PM assayed by MβCD-sampling

A. Transport of newly synthesized ergosterol to the PM at 37°C was measured by withdrawing aliquots of cells from a pulse-chase labeling experiment and sampling PM sterol with MβCD. Data for wild-type and *osh*Δ *osh4-1*^{ts} cells are shown in grey squares and red circles, respectively. The graph shows the amount of [^{3}H]ergosterol in the MβCD extract as a function of time (relative scale, obtained by correcting for the difference in [^{3}H]ergosterol synthesis between wild-type and *osh*Δ *osh4-1*^{ts} cells). The line labeled `IR predicted for *osh*Δ' shows the predicted initial rate of [$^{3}$H]ergosterol accumulation in the MΔCD extract of Osh-deficient cells; the line labeled `IR wt' shows the measured initial rate of [^{3}H]ergosterol accumulation in the MΔCD extract from wild-type cells. See Results and Materials and Methods for further details.

B. Relative specific radioactivity (RSR) calculated as the specific radioactivity of [^{3}H]ergosterol in the MβCD extract divided by the specific radioactivity of [^{3}H]ergosterol in the entire cell. The data correspond to those presented in panel A.

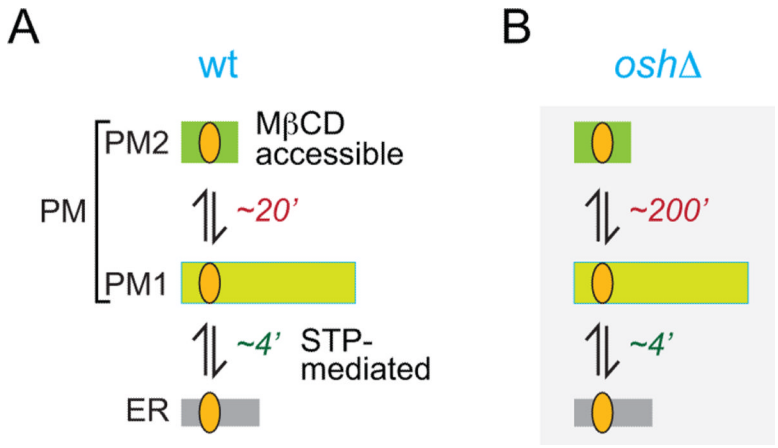

Figure 8. Model for sterol transport between the ER and PM, and compartmentalization of sterols within the PM

See Discussion for details. The times associated with the individual steps are the half-times for transport.

Table 1

Intracellular sterol content of ergosterol- and DHE-loaded cells

Intracellular sterol content (pmol per OD_{600})				
YPD supplement:	**20 mg/L ERG**		**20 mg/L DHE**	
	ERG	**DHE**	**ERG**	**DHE**
*hem1*Δ, 48 hrs	660±50	0	<10	710±40
wt, 36 hrs, hypoxic	730±90	0	140±80	490±170

Table 2

Strains used in this study

Strain	Genotype	Source
Are2Δ	*MAT***a** *are2Δ::KanMX4 his3Δ1 leu2Δ0 ura3Δ0 met15Δ0*	Euroscarf
BY4741	*MAT***a** *his3Δ1 leu2Δ0 ura3Δ0 met15Δ0*	Euroscarf
CBY926	SEY6210 *osh1Δ::KanMX4 osh2Δ::KanMX4 osh3Δ::LYS2 osh4Δ::HIS3 osh5Δ::LEU2 osh6Δ::LEU2 osh7Δ::HIS3* [*TRP1 CEN osh4-1*]	Beh and Rine, 2004 (36)
RH448	*MAT***a** *END4 his4 leu2 ura3 lys2 bar1*	Wylie Nichols
RH1597	*MAT***a** *end4-1 his4 leu2 ura3 lys2 bar1*	Raths et al. 1993 (34)
SEY6210	*MATα leu2-3,112 ura3-52 his3Δ200 trp1-Δ901 lys2-801 suc2Δ9*	Robinson et al. 1988 (67)
YRS1707	*MATα hem1::LEU2 his3Δ1 leu2Δ0 ura3Δ0 lys2Δ0*	Köffel and Schneiter, 2006 (68)